colloids and interfaces

MDPI

Article

Bemotrizinol-Loaded Lipid Nanoparticles for the Development of Sunscreen Emulsions

Maria Grazia Sarpietro [1,2], Debora Santonocito [1,2], Giuliana Greco [1,2], Stefano Russo [3], Carmelo Puglia [1,2] and Lucia Montenegro [1,2,*]

[1] Department of Drug and Health Sciences, University of Catania, 95125 Catania, Italy; mg.sarpietro@unict.it (M.G.S.); debora.santonocito@unict.it (D.S.); giuliana.greco@phd.unict.it (G.G.); capuglia@unict.it (C.P.)
[2] NANOMED—Research Center on Nanomedicine and Pharmaceutical Nanotechnology, University of Catania, 95125 Catania, Italy
[3] Division of Biochemistry, Center for Biomedicine and Medical Technology Mannheim (CBTM), Medical Faculty Mannheim, Heidelberg University, 68159 Mannheim, Germany; stefano.russo@medma.uni-heidelberg.de
* Correspondence: lmontene@unict.it

Abstract

In this work, bemotrizinol (BMTZ), a broad-spectrum UV-filter, was loaded into nanostructured lipid carriers (NLC) whose lipid matrix contained different oils (isopropyl myristate, decyl oleate, caprylic/capric triglyceride) to assess the effects of the lipid core composition on the properties of the resulting NLC. Subsequently, the effects of incorporating different concentrations of optimized BMTZ-loaded NLC on the technological properties of O/W emulsions (pH, viscosity, spreadability, occlusion factor, in vitro BMTZ release, skin permeation, and in vitro sun protection factor) were assessed. The optimized BMTZ-loaded NLC contained 3.0% *w*/*w* of isopropyl myristate and showed mean size = 190.6 ± 9.8 nm, polydispersity index = 0.153 ± 0.013, ζ-potential = −10.6 ± 1.7 mV, and loading capacity = 8% *w*/*w*. The incorporation of increasing concentrations (5, 10, 20% *w*/*w*) of optimized BMTZ loaded into emulsions provided a slight increase in spreadability, lower viscosity, and no change in pH, occlusion factor, and BMTZ release compared to emulsions containing free BMTZ. No BMTZ skin permeation was observed from all formulations. About a 20% increase in sun protection factor values was obtained for vehicles containing BMTZ-loaded NLC compared with formulations incorporating the same amount of free BMTZ. Therefore, incorporating BMTZ-loaded NLC into emulsions could be a promising strategy to develop safer and more effective sunscreen formulations.

Keywords: bemotrizinol; nanostructured lipid carriers; sunscreens; emulsions; organic UV-filters

Academic Editors: César Burgos-Díaz, Carla Arancibia, Karla Garrido-Miranda, Julia Maldonado-Valderrama and Reinhard Miller

Received: 30 June 2025
Revised: 14 August 2025
Accepted: 22 August 2025
Published: 26 August 2025

Citation: Sarpietro, M.G.; Santonocito, D.; Greco, G.; Russo, S.; Puglia, C.; Montenegro, L. Bemotrizinol-Loaded Lipid Nanoparticles for the Development of Sunscreen Emulsions. *Colloids Interfaces* **2025**, *9*, 54. https://doi.org/10.3390/colloids9050054

1. Introduction

Nowadays, organic (chemical) and inorganic (physical) UV-filters play a fundamental role in preventing the deleterious effect of skin exposure to solar radiation, such as erythema, sunburns, actinic keratosis, cutaneous carcinoma, and melanoma [1–3]. Nevertheless, their safety, both for humans and environment, has been repeatedly questioned [4–6]. To improve sunscreen products' efficacy and safety, several researchers have proposed the incorporation of organic UV-filters into lipid nanoparticles because of the capability of these nanocarriers to reflect solar radiation, thus behaving as physical sunscreens. The resulting

synergic effect of physical sunscreen (lipid nanoparticles) and an organic UV-filter allows for reducing the amount of organic UV-filter required to achieve the desired photoprotection [7–11]. A recent investigation clearly demonstrated a photoprotection improvement due to loading organic UV-A and UV-B filters into nanostructured lipid carriers while decreasing the content of organic filters and providing vehicles with suitable technological properties [11]. In addition, Sharma et al. [12] pointed out that lipid nanoparticles could also be regarded as suitable carriers for natural sunscreen agents such as green tea extracts. Lipid nanoparticles, namely, solid lipid nanoparticles (SLN) and nanostructured lipid carriers (NLC), have been reported to be promising candidates as topical delivery systems [13,14]. Their advantages encompass controlled release of the incorporated active ingredients, high tolerability and biocompatibility, safety, ability to modulate drug skin penetration/permeation, and improvement of skin hydration because of their occlusive properties, resulting from their lipid content [15–18]. Indeed, the composition of the lipid matrix is the main feature that differentiates SLN from NLC, as both types of nanoparticles are made up of a lipid core stabilized by different types of surfactants in aqueous media [19,20]. In particular, the lipid core of SLN, the first generation of lipid nanoparticles, consists of solid lipids, whose highly ordered arrangement leads to poor drug incorporation and drug leakage during storage. These drawbacks were overcome by developing a second generation of lipid nanoparticles, such as NLC, using mixtures of solid and liquid lipids as a nanoparticle matrix, thus increasing both the stability and drug loading ability of the resulting colloidal systems.

In recent years, the increasing knowledge of the harmful effects of skin exposure to UV-A radiation and the limited availability of safe organic UV-filters effective in absorbing UV-A rays have prompted researchers to focus on the development of sunscreen products with improved photoprotective activity against UV-A.

Bemotrizinol (BMTZ) has been marketed as a broad-spectrum sunscreen agent due to its ability to absorb UV radiation in the range of 280–380 nm [21,22]. As the incorporation of BMTZ into NLC could offer the advantage of improving the SPF value of a sunscreen formulation without increasing the amount of chemical UV-filter incorporated, Medeiros et al. [23] investigated the ability of NLC consisting of carnauba wax as solid lipid and caprylic/capric triglycerides as liquid lipid to load BMTZ. The authors demonstrated an improvement in the in vitro photoprotective activity of BMTZ-loaded NLC in comparison with free BMTZ, but they did not evaluate the effects of incorporating BMTZ-loaded NLC into sunscreen formulations. In addition, these authors performed their investigation using a single combination of solid lipid and liquid lipid. However, several studies pointed out that SLN and NLC show different technological properties depending on the used lipids and the ratio of solid/liquid lipids, which, in turn, could affect their ability to improve the efficacy and safety of the loaded active ingredients [24–26].

In this context, this work aimed to assess the effects of different lipid core compositions on the physicochemical characteristics of BMTZ-loaded NLC to design new sunscreen formulations with suitable technological properties. NLC were obtained by the phase inversion temperature (PIT) method, which could allow for easy formulation scaling up, as it did not require specific equipment or special operating conditions [27]. After choosing the ratio of solid/liquid lipid that provided NLC with a small particle size and low polydispersity index (PDI), different percentages of BMTZ (1, 3, 5, 7% *w*/*w*) were incorporated into such NLC. The thermal behavior of the resulting nanocarriers was investigated using differential scanning calorimetry (DSC) to gain information about the BMTZ location in the nanoparticles.

As products intended for topical application should have suitable technological properties depending on their specific use, lipid nanoparticles are often incorporated in semisolid dosage forms such as gels and creams [28]. However, as reported by Safta et al. [28], the addition of lipid nanoparticles to semisolid vehicles could alter some properties of the resulting formulations, such as stability, viscosity, texture, pH, and spreadability. As creams are the most commonly used sunscreen formulations, a further aim of this study was to assess the effects of incorporating BMTZ-loaded NLC into topical emulsions. Therefore, the optimized BMTZ-loaded NLC were added, at different concentrations, to an O/W emulsion, and the technological properties (pH, viscosity, spreadability, occlusion factor, BMTZ in vitro release, skin permeation, and in vitro sun protection factor) of the resulting formulations were evaluated.

2. Materials and Methods

2.1. Materials

The following liquid lipids were used: isopropyl myristate (IPM, Galeno—Carmignano, Prato, Italy), decyl oleate (Cetiol V®, DO, BASF—Ludwigshafen, Germany), and caprylic/capric triglyceride (Myritol 318®, MYR, BASF—Ludwigshafen, Germany). Cetyl palmitate (Cutina CP®, CP, BASF—Ludwigshafen, Germany) was used as a solid lipid. Galeno (Carmignano, Prato, Italy) supplied imidazolidinyl urea (Kemipur 100®) and benzyl alcohol as preservatives and disodium EDTA (EDTA) as a chelating agent. Diethylhexylcyclohexane (Cetiol S®) and bis-ethylhexyloxyphenol methoxyphenyl triazine (bemotrizinol, Tinosorb S®, BMTZ) were a kind gift from BASF (Ludwigshafen, Germany). Steareth-2 (Brij 72®), steareth-21 (Brij 721®), and oleth-20 (Brij 98®) were provided by Sigma-Aldrich (Milan, Italy). Glyceryl oleate (Tegin O®, GO) was obtained from A.C.E.F. S.p.A. (Fiorenzuola D'Arda-Piacenza, Italy). Cetyl alcohol and tocopheryl acetate (TA) were purchased from Farmalabor (Canosa di Puglia, Bari, Italy). Argan oil was purchased from Makeitlab (Barletta, Italy). Triticum vulgare germ oil (Wheat oil), and coconut alkanes (and) coco-caprylate/caprate (Greensyl®) were supplied by Camelis (Parma, Italy). Butyrospermum Parkii oil (Shea Oil), and cetearyl ethylhexanoate (and) isopropyl myristate (Crodamol® CAP) were obtained from Aroma-Zone (Paris, France). Parfum was kindly donated by Muller and Koster (Liscate, Milan, Italy).

2.2. Preparation of Nanostructured Lipid Carriers (NLC)

The composition of the investigated NLC is reported in Tables 1 and 2. All nanocarriers were prepared by the phase inversion temperature (PIT) method, as reported in previous works [29,30]. Briefly, the oil phase (containing different percentages of BMTZ when BMTZ-loaded NLC were prepared) and aqueous phase were heated at about 90 °C, separately. The aqueous phase consisted of deionized water to which Kemipur 100® 0.35% *w*/*w* was added as a preservative. The aqueous phase was slowly poured into the oil phase under continuous stirring (700 rpm). The resulting formulation was stirred until room temperature was achieved. At the PIT, the sample turned clear. All samples were stored sheltered from light at room temperature.

Table 1. Composition (% *w*/*w*) of the lipid phase of unloaded nanostructured lipid carriers (NLC) containing different percentages of lipids.

NLC Code	Oleth-20	GO [a]	CP [b]	IPM [c]	MYR [d]	DO [e]
IPM1	8.7	4.4	6.0	1.0	---	---
IPM2	8.7	4.4	5.0	2.0	---	---
IPM3	8.7	4.4	4.0	3.0	---	---
MYR1	8.7	4.4	6.0	---	1.0	---
MYR2	8.7	4.4	5.0	---	2.0	---
MYR3	8.7	4.4	4.0	---	3.0	---
DO1	8.7	4.4	6.0	---	---	1.0
DO2	8.7	4.4	5.0	---	---	2.0
DO3	8.7	4.4	4.0	---	---	3.0

[a] GO = glyceryl oleate; [b] CP = cetyl palmitate; [c] IPM = isopropyl myristate; [d] MYR = caprylic/capric triglyceride; [e] DO = decyl oleate.

Table 2. Composition (% *w*/*w*) of the lipid phase of nanostructured lipid carriers (NLC) containing different percentages of bemotrizinol.

NLC Code	Oleth-20	GO [a]	CP [b]	IPM [c]	MYR [d]	DO [e]	BMTZ [f]
IBMTZ1	8.7	4.4	4.0	3.0	---	---	1.0
IBMTZ3	8.7	4.4	4.0	3.0	---	---	3.0
IBMTZ5	8.7	4.4	4.0	3.0	---	---	5.0
IBMTZ7	8.7	4.4	4.0	3.0	---	---	7.0
MBMTZ1	8.7	4.4	4.0	---	3.0	---	1.0
MBMTZ3	8.7	4.4	4.0	---	3.0	---	3.0
MBMTZ5	8.7	4.4	4.0	---	3.0	---	5.0
MBMTZ7	8.7	4.4	4.0	---	3.0	---	7.0
DBMTZ1	8.7	4.4	4.0	---	---	3.0	1.0
DBMTZ3	8.7	4.4	4.0	---	---	3.0	3.0
DBMTZ5	8.7	4.4	4.0	---	---	3.0	5.0
DBMTZ7	8.7	4.4	4.0	---	---	3.0	7.0

[a] GO = glyceryl oleate; [b] CP = cetyl palmitate; [c] IPM = isopropyl myristate; [d] MYR = caprylic/capric triglyceride; [e] DO = decyl oleate; [f] BMTZ = bemotrizinol.

2.3. Characterization of Unloaded and Bemotrizinol-Loaded NLC

Transmission electron microscopy (TEM) was used to analyze NLC morphology. Briefly, 5 µL of the sample was placed on a Formvar (200-mesh) copper grid (TAAB Laboratories Equipment, Berks, UK). After removing the excess of the sample by filter paper, a drop of uranyl acetate (2% *w*/*w* in water) was added. After drying at room temperature, the sample was analyzed by a transmission electron microscope (model JEM 2010, Jeol, Peabody, MA, USA), which operated at an acceleration voltage of 200 KV.

NLC particle size and distribution (polydispersity index, PDI) were assessed by dynamic light scattering (Zetasizer Nano ZS90, Malvern Instruments, Malvern, UK). Shortly, measures were performed using a 4 mW laser diode at 670 nm and scattering light at 90°. All analyses were carried out after diluting the sample (1:5, sample/distilled water) and letting it settle down to 25 °C for 2 min. Values were reported based on intensity and expressed as Z-average. The same instrument (Zetasizer Nano ZS90) was used to assess ζ-potential by laser Doppler velocimetry. All samples were diluted with KCl 1 mM (pH 7.0) before analysis.

2.4. Differential Scanning Calorimetry (DSC) Analyses

A Mettler Toledo STAR^e thermoanalytical system (Greifensee, Switzerland) was used to perform DSC analyses. The instrument was equipped with a DSC822 calorimetric cell. Calorimetric data were analyzed by the Mettler STAR^e software (version 16.00) (Greifensee, Switzerland). Indium (99.95%) was used to calibrate the instrument whose sensitivity was automatically set as the maximum by the calorimeter itself. Freshly prepared NLC samples (80 µL) were put into aluminum calorimetric pan, which was sealed and analyzed as follows: to the following scans: a scan from 10 to 60 °C (4 °C/min); an isotherm at 60 °C (4 min); a scan from 60 to 10 °C (4 °C/min); an isotherm at 10 °C (4 min). The procedure was repeated three times. All analyses were performed under N_2 flow (70 mL/min). The enthalpy variation (ΔH) was calculated by integrating the area under the transition peak, and the percentage of recrystallization index (RI) was calculated according to Equation (1) [31]:

$$RI\% = \frac{\Delta H_{nanoparticles}}{\Delta H_{bulk\ material} \times concentration_{lipid\ phase}} \times 100 \quad (1)$$

2.5. Stability Studies on Nanostructured Lipid Carriers (NLC)

The stability of all NLC samples was evaluated during storage for two months at controlled room temperature (20 ± 1 °C) and sheltered from light. At specified intervals (24 h, 1 week, 1 month, 2 months), samples were withdrawn and analyzed to determine particle sizes, PDI, and ζ-potential values. Analyses were performed only on samples that did not show any sign of precipitation. Each measurement was performed in triplicate.

2.6. Preparation of O/W Emulsions

The composition of O/W emulsions containing free BMTZ or BMTZ-loaded NLC is illustrated in Table 3.

Phases A and B were heated separately to 70 °C. Then, the aqueous phase was poured into the oil phase under vigorous stirring (Turbomixer Silverson SL2, Silverson Machines Inc., East Longmeadow, MA, USA). After the emulsifying process, the formulation was cooled to 40 °C under slow and continuous stirring. At this temperature, phase C and phase D were added. Afterward, the required amount of BMTZ-loaded NLC (phase E) was added to samples B_{NLC}, C_{NLC}, and D_{NLC}, during mixing. The resulting formulation was cooled to room temperature without stopping the stirring. The pH of each formulation was determined 48 h after its preparation to allow it to settle down. Prior to performing, at room temperature, the pH measurement by a Crison pH-meter model Basic 20 (Crison Instruments, Barcelona, Spain), and each sample was diluted to one-tenth of its original concentration using distilled water [32].

2.7. Stability Studies on O/W Emulsions

All O/W emulsions were stored at room temperature for three months, sheltered in the dark. At specified intervals (48 h, 1 week, 2 weeks, 1 month, 2 months, 3 months), samples were evaluated by determining their appearance, pH, and viscosity.

2.8. Spreadability

The parallel-plate method was used to assess sample spreadability, as previously reported [33,34]. Each sample (1 g) was placed between two 20 × 20 cm glass plates, and a 200 g weight was put on the upper plate. The weight was removed after 1 min. and the spreading diameter (expressed in centimeters) was determined. Each experiment was performed in triplicate.

Table 3. Composition (expressed as % *w*/*w*) of formulations containing bemotrizinol-free and bemotrizinol-loaded nanostructured lipid carriers (NLC).

Ingredient	Formulation Code						
	A	B	B_{NLC}	C	C_{NLC}	D	D_{NLC}
Phase A							
Cetiol S [a]	3.0	3.0	3.0	3.0	3.0	3.0	3.0
MYR [b]	2.0	2.0	2.0	2.0	2.0	2.0	2.0
Greensyl [c]	1.0	1.0	1.0	1.0	1.0	1.0	1.0
Crodamol CAP [d]	2.0	2.0	2.0	2.0	2.0	2.0	2.0
Argan oil	1.0	1.0	1.0	1.0	1.0	1.0	1.0
Wheat oil	1.0	1.0	1.0	1.0	1.0	1.0	1.0
Shea oil	1.0	1.0	1.0	1.0	1.0	1.0	1.0
TA [e]	0.1	0.1	0.1	0.1	0.1	0.1	0.1
Brij 72 [f]	3.0	3.0	3.0	3.0	3.0	3.0	3.0
Brij 721 [g]	2.0	2.0	2.0	2.0	2.0	2.0	2.0
Cetyl palmitate	4.0	4.0	4.0	4.0	4.0	4.0	4.0
Cetyl alcohol	1.0	1.0	1.0	1.0	1.0	1.0	1.0
BMTZ [h]	---	0.4	---	0.8	---	1.6	---
Phase B							
EDTA [i]	0.1	0.1	0.1	0.1	0.1	0.1	0.1
Water	q.s. [l]	q.s. [l]	q.s. [l]	q.s. [l]	q.s. [l]	q.s. [l]	q.s. [l]
Phase C							
Kemipur 100 [m]	0.35	0.35	0.35	0.35	0.35	0.35	0.35
Benzyl alcohol	0.25	0.25	0.25	0.25	0.25	0.25	0.25
Phase D							
Parfum	0.1	0.1	0.1	0.1	0.1	0.1	0.1
Phase E							
BMTZ-NLC [n]	---	---	5.0	---	10.0	---	20.0

[a] Cetiol S = diethylhexylcyclohexane; [b] MYR = caprylic/capric triglyceride; [c] Greensyl = coconut alkanes and coco-caprylate/caprate; [d] Crodamol CAP = cetearyl ethylhexanoate and isopropyl myristate; [e] TA = tocopheryl acetate; [f] Brij 72 = Steareth-2; [g] Brij 721 = Steareth-21; [h] BMTZ = bemotrizinol; [i] EDTA = disodium EDTA; [l] q.s. = quantum sufficit to 100% *w*/*w*; [m] Kemipur 100 = imidazolidinyl urea; [n] BMTZ-NLC = bemotrizinol-loaded nanostructure lipid carriers.

2.9. Occlusive Properties

The occlusion factor of the investigated formulations was assessed, as previously described [35,36]. Briefly, beakers (100 mL) filled with 50 mL of distilled water were used. Each beaker was covered with filter paper (cellulose acetate filter, perfecte 2, 90 mm, cut-off size: 4–7 µm, Cartiera Cordenons, Pordenone, Italy) and sealed. After spreading the formulation evenly (200 mg) on the filter surface (18.8 cm^2; applied amount 10.6 mg/cm^2), the samples were accurately weighted and stored at 32 °C (skin surface temperature) for 48 h (50–55% RH) in an incubator (Incubator IN 30, Memmert GmbH, Schwabach, Germany). After this period, water evaporation through the filter paper was determined by weighing each sample. The water loss from beakers covered with filter paper but free of the sample formulation was used as a reference. The occlusion factor (F) was calculated according to Equation (2):

$$F = 100 \times [(A - B)/A] \quad (2)$$

where A is the water loss from beakers without the sample (reference) and B is the water loss with the sample. Each experiment was performed in triplicate.

2.10. Viscosity

The viscosity of all emulsions was determined 48 h after their preparation [37]. Measurements were performed using a Brookfield DV-II + Pro viscometer (Brookfield Engineering Laboratories, Inc., Middleboro, MA, USA) equipped with the spindle number 6 at 25 ± 0.5 °C and 6 rpm. The instrument was calibrated according to the instructions provided by the manufacturer using silicone oil as the standard fluid. Analyses were performed 1 h after placing the sample in the instrument. Each determination was performed in triplicate, and the results were expressed in cPs.

2.11. In Vitro Release of Bemotrizinol

BMTZ release rate from the O/W emulsions was determined according to a procedure described previously [29,38]. Briefly, Franz-type diffusion cells (LGA, Berkeley, CA, USA) were used, and BMTZ release was assessed through cellulose membranes that were immersed in distilled water for 1 h at room temperature prior to performing the experiment (surface area available for diffusion: 0.75 cm^2, receptor volume: 4.5 mL). For ensuring pseudo-sink conditions, a mixture consisting of water/ethanol (50/50 v/v) was used as the receiving phase [29] and was constantly stirred (700 rpm) and thermostated at 35 °C to maintain the membrane surface at 32 °C. After applying the sample (2 mg/cm^2) on the membrane surface, aliquots of the receptor phase (600 µL) were withdrawn at specified intervals (0, 30, 60, 90, 120, 240 min) and replaced with an equal volume of water/ethanol (50/50 v/v) pre-thermostated to 35 °C. BMTZ content in the receiving solution samples was determined spectrophotometrically (UV-VIS Spectrophotometer Shimadzu model UV-1601, Shimadzu Italia, Milan, Italy) at 340 nm. Quantitative analyses were performed using a calibration curve in the range 0.1–10.0 µg/mL (limit of detection 0.01 µg/mL, limit of quantification 0.05 µg/mL). Each experiment was performed in triplicate.

2.12. In Vitro Skin Permeation Experiments

Skin permeation experiments through excised human skin were performed as previously reported [4]. In vitro experiments were performed on stratum corneum and epidermis (SCE) membranes because, in vitro, the dermis could behave as an additional barrier to the penetration of lipophilic compounds, such as BMTZ. Briefly, SCE membranes were prepared from adult (mean age 35 ± 9 years) human skin samples obtained from abdominal plastic surgery. The subcutaneous fat was trimmed, and the resulting skin samples were immersed in distilled water at 60 ± 1 °C for 2 min. Then, SCE membranes were removed from the dermis using a scalpel blade. The resulting SCE samples were dried in a desiccator (25% RH) and stored at 4 ± 1 °C for a period not exceeding three months. One hour prior to starting the experiment, SCE samples were immersed in distilled water at room temperature to rehydrate. SCE samples were placed in the same Franz-type diffusion cells described above. SCE samples were assessed for barrier integrity by measuring in vitro permeability coefficient of [3H] water under the same experimental conditions used for in vitro permeation experiments, as previously reported [4]. The value of the permeability coefficient for tritiated water was $1.8 \pm 0.2 \times 10^{-3}$, which was in the accepted range for samples with normal skin permeability [4]. In vitro skin permeation experiments were carried out under the same experimental conditions reported for in vitro release studies. To evaluate potential analytical interferences due to the release of skin components in the receiving phase, preliminary experiments were performed in the same experimental conditions described for in vitro skin permeation studies, but without adding any formulation in the donor compartment. All samples withdrawn from the receiving phase did not show any absorbance at 340 nm (the absorbance length at which BMTZ was analyzed). Therefore, any

interference due to the release of skin components in the receptor medium was excluded. Each formulation was analyzed in triplicate on three different skin specimens.

2.13. In Vitro Sun Protection Factor (SPF)

In vitro sun protection factor (SPF) values of O/W emulsions containing free NLC or NLC loaded with BMTZ were calculated according to the method described by Mansur et al. [39], with minor modifications. Each sample was properly diluted in deionized water (final concentration 200 µg/mL) and analyzed spectrophotometrically (UV-VIS Spectrophotometer Shimadzu mod. UV-1601, Shimadzu Italia, Milan, Italy), acquiring absorption data every 5 nm in the range of 290–320 nm. SPF values were determined according to the following Equation (3):

$$\mathrm{SPF}_{\mathrm{spectrophotometric}} = \mathrm{CF} \times \sum_{290}^{320} \mathrm{EE}(\lambda) \times \mathrm{I}(\lambda) \times \mathrm{Abs}(\lambda) \quad (3)$$

where CF = correction factor (=10); EE(λ) = erythemal effect of the radiation with wavelength λ; I(λ) = solar intensity of radiation with wavelength λ; Abs(λ) = absorbance of the sunscreen at wavelength λ. To calculate the SPF of each formulation, the values of EE(λ) × I(λ) at each wavelength in the range of 290–320 nm, determined by Ricci et al. [40], were used.

2.14. Statistical Analysis

For all measurements, mean values ± standard deviation (S.D.) were calculated. Statistical analyses were performed using Student's *t*-test after checking data normality. Values were considered statistically different when $p < 0.05$.

3. Results and Discussion

Mixtures containing different ratios of solid and liquid lipids were assessed to prepare BMTZ-loaded NLC. Cetyl palmitate (CP) was used as a solid lipid, while caprylic/capric triglyceride (MYR), isopropyl myristate (IPM) and decyl oleate (DO) were investigated as liquid lipids. All lipids were chosen due to their wide use and safety as cosmetic ingredients [41,42]. All NLC contained the same total amount of lipids (7% *w*/*w*) but different solid/liquid lipid ratios, namely, 6%/1%, 5%/2%, and 4%/3%. The choice of the total amount of lipid was based on previous studies performed on NLC containing a mixture of cetyl palmitate and IPM as the lipid matrix, showing that a 7% *w*/*w* total amount of lipid allowed for obtaining NLC with better technological properties [29]. Unloaded NLC were coded according to the following criteria: for NLC containing isopropyl myristate, the code IPM was used; for NLC containing caprylic/capric triglyceride, the code MYR was used; for NLC containing decyl oleate, the code DO was used; NLC containing 1% *w*/*w* of liquid lipid were coded using the number 1; NLC containing 2% *w*/*w* of liquid lipid were coded using the number 2; NLC containing 3% *w*/*w* of liquid lipid were coded using the number 3. The morphology of such nanocarriers (unloaded and BMTZ-loaded NLC) was assessed by TEM, which showed roughly spherical nanoparticles with no significant sign of aggregation. As all NLC provided similar TEM images, pictures obtained from only one sample of unloaded NLC containing IPM 3.0% *w*/*w* and the corresponding NLC loaded with BMTZ 1% *w*/*w* are shown in Figure 1.

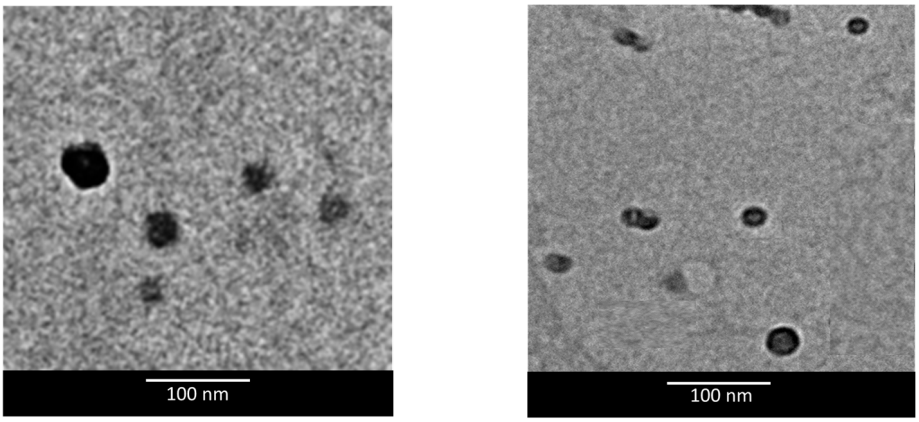

(**a**) (**b**)

Figure 1. TEM (transmission electron microscopy) pictures of (**a**) nanostructured lipid carriers prepared using isopropyl myristate 3.0% *w*/*w* and (**b**) nanostructured lipid carriers prepared using isopropyl myristate 3.0% *w*/*w* and bemotrizinol 1% *w*/*w* loading.

With regard to unloaded NLC, mean particle sizes ranged from 37.4 to 48.1 nm, and PDI values were well below 0.300 (see Table 4), thus confirming the ability of the phase inversion temperature (PIT) method to provide lipid nanoparticles with small mean sizes and narrow size distribution, as previously reported [29,30]. For all unloaded NLC, no significant relationship was observed between the percentage of liquid lipid and the mean size of the resulting nanoparticles. Among the investigated liquid lipids, IPM led to nanoparticles with smaller mean size compared to MYR and DO while no relevant difference was observed comparing PDI and ζ-potential values. The smaller mean size of NLC obtained using IPM could be due to stronger interactions between the lipid core and the surfactant/co-surfactant layer resulting in smaller curvature radius of the nanoparticles [43].

Table 4. Mean nanoparticle size (Z-average ± S.D.), polydispersity index (PDI ± S.D.), and ζ potential (Zeta ± S.D.) of unloaded nanostructured lipid carriers (NLC).

NLC Code	Z-Average ± S.D. (nm)	PDI	Zeta ± S.D. (mV)
IPM1	38.5 ± 1.5	0.102 ± 0.008	−10.3 ± 1.1
IPM2	37.4 ± 1.8	0.111 ± 0.007	−9.2 ± 1.2
IPM3	37.9 ± 2.0	0.107 ± 0.011	−11.3 ± 0.9
MYR1	47.9 ± 2.8	0.115 ± 0.008	−8.9 ± 1.0
MYR2	45.6 ± 1.6	0.105 ± 0.009	−10.4 ± 1.7
MYR3	48.1 ± 1.9	0.109 ± 0.007	−9.4 ± 0.8
DO1	45.3 ± 1.4	0.153 ± 0.009	−11.5 ± 1.6
DO2	41.1 ± 2.0	0.171 ± 0.012	−9.9 ± 1.2
DO3	41.7 ± 2.3	0.166 ± 0.008	−10.6 ± 1.8

To better elucidate the mechanisms involved in the production of NLC with different mean sizes, DSC studies were performed on both unloaded and BMTZ-loaded NLC. DSC is a widely used technique to characterize lipid nanocarriers that provides useful information about the interactions occurring among the NLC components [44]. In particular, parameters involved in NLC stability and drug loading ability, such as lipid modifications and crystallinity degree, can be studied using DSC. Indeed, during the cooling step in the NLC preparation process, lipids could crystallize in the following polymorphic forms: α, thermodynamically unstable, β′, metastable, and β, stable [45]. In our study, we used as solid lipid cetyl palmitate, which shows two endothermic peaks (Figure S1), at about 39 and 50 °C due, respectively, to the fusion of the α and β forms [31,46].

The calorimetric curves of NLC containing different amounts of DO, IPM, and MYR (Figure 2a, Figure 2b, and Figure 2c, respectively) pointed out that the presence of a liquid lipid in the NLC core led to a decrease in both the transition temperature (Tm) and the peak intensity (ΔH) as the percentage of liquid lipid increased. A similar depression of the calorimetric parameters has been already reported by others [47] studying the effects of increasing the concentrations of MYR in the solid lipid core of SLN.

To understand if the decrease in the peak temperature and intensity was due to the lower amount of cetyl palmitate or to the increase in liquid lipid in the NLC core, solid lipid nanoparticles (SLN) containing 6% or 5% *w*/*w* cetyl palmitate were prepared (using the same procedure described to obtain unloaded NLC) and analyzed using DSC. Cetyl palmitate amounts lower than 5% *w*/*w* were not tested, as they did not lead to SLN formation. As shown in Figure 3, the peak intensity of SLN containing 6% *w*/*w* or 5% *w*/*w* cetyl palmitate was quite similar but the Tm value of SLN containing 5% cetyl palmitate was smaller than that of SLN containing 6% cetyl palmitate. A reduction in the melting temperature by decreasing the amount of cetyl palmitate in the SLN matrix has already been reported and it has been attributed to a lower crystallization and a faster transition from the instable α form to the stable β form after crystallization [48]. However, although the amount of cetyl palmitate used to prepare the lipid nanoparticles affected the transition temperature and the peak intensity, the effect was not as pronounced as that due to the amount of liquid lipid. Therefore, the decrease in ΔH and Tm values seemed to be due, mainly, to the content of liquid lipid rather than to the amount of solid lipid contained in the lipid core.

As shown in Figure 4, a pseudo-linear relationship between the transition temperatures of unloaded NLC and the percentage of liquid lipid in the NLC core was observed as the higher the liquid lipid percentage means the lower the melting temperature, regardless of the type of liquid lipid used. However, the reduction in Tm values due to the increase in liquid lipid content was more pronounced in the NLC containing IPM followed by DO and, then, by MYR.

As mentioned above, during the cooling step of the NLC preparation process, lipids can crystallize in different polymorphic forms. In thermodynamically unstable forms, lipid molecules show higher mobility and higher ability to incorporate drugs. As reported in the literature [31], the enthalpy variation (ΔH) is closely related to the system crystallinity: a reduction in the enthalpy variation indicates a less ordered and, thus, less crystalline structure. However, the different type of liquid lipid used could affect the crystallinity of the system. The data illustrated in Table 5 point out an inverse correlation between the recrystallization index (RI) and the percentage of liquid lipid in the NLC matrix as an increase in liquid lipid content led to a reduction in RI. This trend was observed for all investigated oils but no relationship was detected between oil lipophilicity and RI values. As lower NLC matrix crystallinity is thought to allow higher active ingredient loading [31,47], NLC showing the lowest RI values (3% *w*/*w* liquid lipid) were chosen to load the sunscreen agent BMTZ. BMTZ-loaded NLC were coded according to the following criteria: for NLC containing isopropyl myristate, the code I was used; for NLC containing caprilic/capric triglyceride, the code M was used; for NLC containing decyl oleate, the code D was used; NLC containing 1%, 3%, 5%, and 7% *w*/*w* BMTZ were coded as BMTZ1, BMTZ3, BMTZ5, and BMTZ7, respectively. BMTZ calorimetric curve is depicted in Figure S2, showing an endothermic peak at 78 °C.

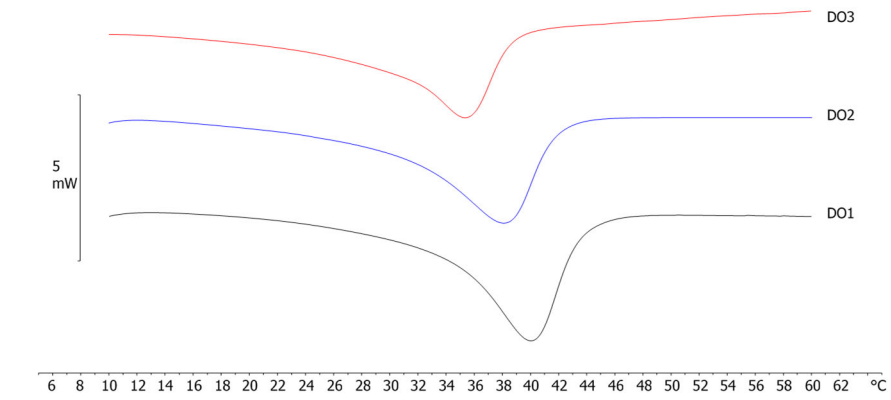

(**a**)

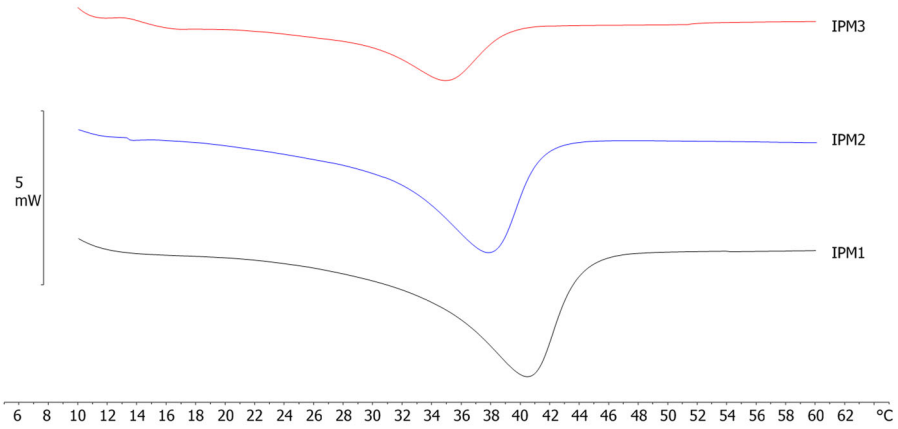

(**b**)

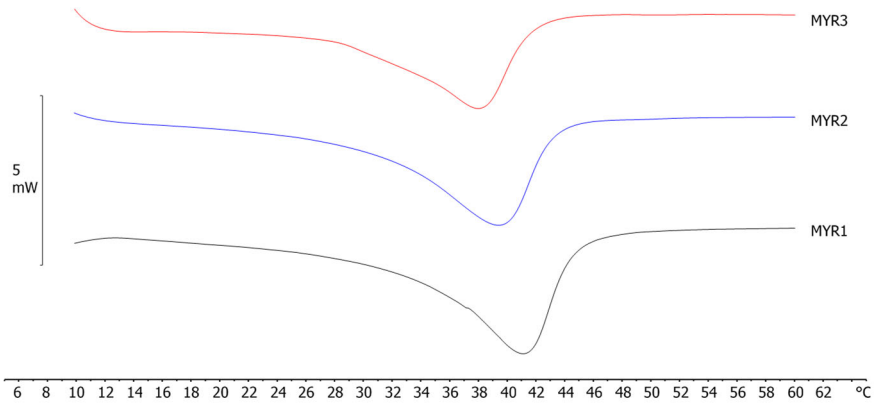

(**c**)

Figure 2. Curves obtained by differential scanning calorimetry of nanostructured lipid carriers prepared with different percentages of (**a**) decyl oleate (1% *w*/*w* = DO1, 2% *w*/*w* = DO2, 3% *w*/*w* = DO3), (**b**) isopropyl myristate (1% *w*/*w* = IPM1, 2% *w*/*w* = IPM2, 3% *w*/*w* = IPM3), and (**c**) caprylic/capric triglyceride (1% *w*/*w* = MYR1, 2% *w*/*w* = MYR2, 3% *w*/*w* = MYR3). Each experiment was performed in triplicate (n = 3).

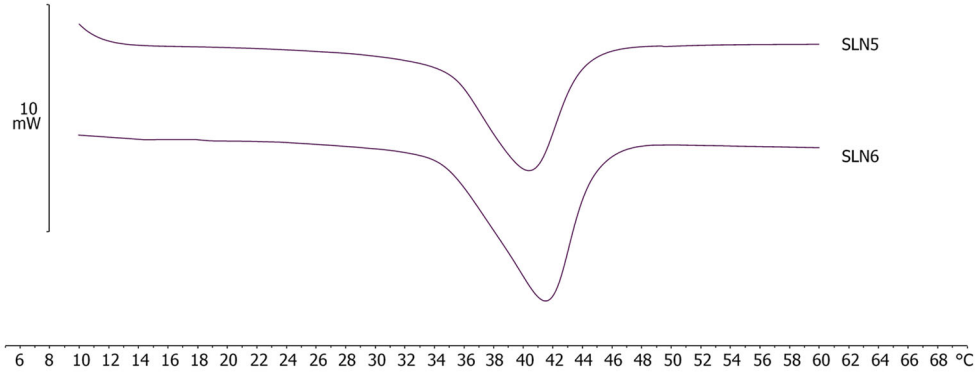

Figure 3. Curves obtained by differential scanning calorimetry of solid lipid nanoparticles (SLN) containing cetyl palmitate 5% *w*/*w* (SLN5) and 6% *w*/*w* (SLN6).

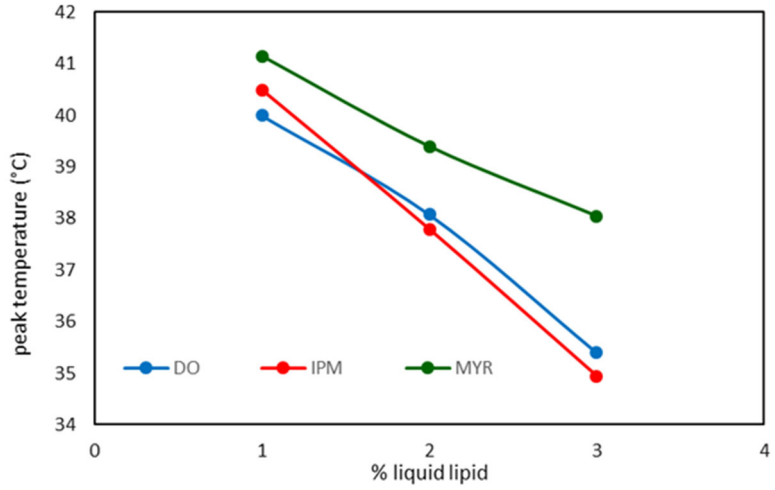

Figure 4. Transition temperature of the main peak of nanostructured lipid carriers (NLC) as a function of the percentage of liquid lipid content in the NLC core. Transition temperature data were obtained from experiments performed in triplicate (n = 3) and their S.D. was within 1%. DO = decyl oleate; IPM = isopropyl myristate; MYR = caprilic/capric triglyceride.

Table 5. Enthalpy variation (ΔH) and recrystallization index (RI %) of unloaded nanostructured lipid carriers (NLC) containing different percentages of liquid lipids.

NLC Code	ΔH ± S.D. (J/g)	RI %
DO 1	9.46 ± 0.38	63.9
DO 2	7.22 ± 0.14	58.5
DO 3	5.01 ± 0.05	50.8
IPM 1	8.96 ± 0.24	60.5
IPM 2	6.59 ± 0.20	53.4
IPM 3	2.23 ± 0.08	22.6
MYR 1	10.37 ± 0.45	70.0
MYR 2	7.80 ± 0.15	63.0
MYR 3	4.21 ± 0.17	42.6

As shown in Table 6, raising the percentage of BMTZ incorporated into the NLC the mean size of the nanoparticles increased, regardless of the type of liquid lipid used to prepare the colloidal carriers. All BMTZ-loaded NLC showed PDI values lower than 0.300, thus pointing out that such colloidal systems were monodispersed.

Table 6. Mean nanoparticle size (Z-average ± S.D.), polydispersity index (PDI ± S.D.), and ζ potential (Zeta ± S.D.) of bemotrizinol-loaded nanostructured lipid carriers (NLC).

NLC Code	Z-Average ± S.D. (nm)	PDI	Zeta ± S.D. (mV)
IBMTZ1	33.2 ± 2.1	0.217 ± 0.015	−10.4 ± 1.3
IBMTZ3	35.5 ± 1.9	0.090 ± 0.004	−9.9 ± 1.7
IBMTZ5	45.3 ± 2.3	0.115 ± 0.009	−11.8 ± 1.4
IBMTZ7	72.5 ± 6.3	0.149 ± 0.014	−9.9 ± 1.3
MBMTZ1	49.8 ± 2.9	0.127 ± 0.011	−11.2 ± 1.4
MBMTZ3	58.4 ± 2.1	0.136 ± 0.009	−10.2 ± 1.9
MBMTZ5	78.1 ± 3.9	0.191 ± 0.018	−11.5 ± 0.9
MBMTZ7	99.3 ± 2.5	0.289 ± 0.019	−9.9 ± 1.2
DBMTZ1	45.0 ± 4.1	0.129 ± 0.013	−10.7 ± 1.5
DBMTZ3	50.8 ± 4.3	0.167 ± 0.015	−11.2 ± 1.4
DBMTZ5	66.9 ± 3.3	0.181 ± 0.018	−11.3 ± 1.8
DBMTZ7	81.5 ± 2.8	0.264 ± 0.019	−10.8 ± 0.7

Calorimetric curves of NLC containing 3% *w*/*w* of liquid lipid and different percentages of BMTZ are depicted in Figure 5a–c. The incorporation of BMTZ into NLC in-fluenced the thermal behavior of the resulting colloidal systems, depending on the type of liquid lipid used.

Regarding NLC prepared using DO as oil, a shift in the calorimetric peak toward higher temperatures was observed as the amount of BMTZ loaded into the NLC increased (Figure 5a). It is worth noting that at low percentage of BMTZ (1–3% *w*/*w*), a single peak was present; at 5% *w*/*w* BMTZ, the main peak was preceded by a large shoulder, while at 7% BMTZ, two distinct peaks were observed. This behavior suggests that BMTZ, up a certain amount, distributed uniformly into the NLC structure, whereas at high amounts, regions rich in compound and regions poor in compound coexisted in the NLC structure, as indicated by the presence of two peaks.

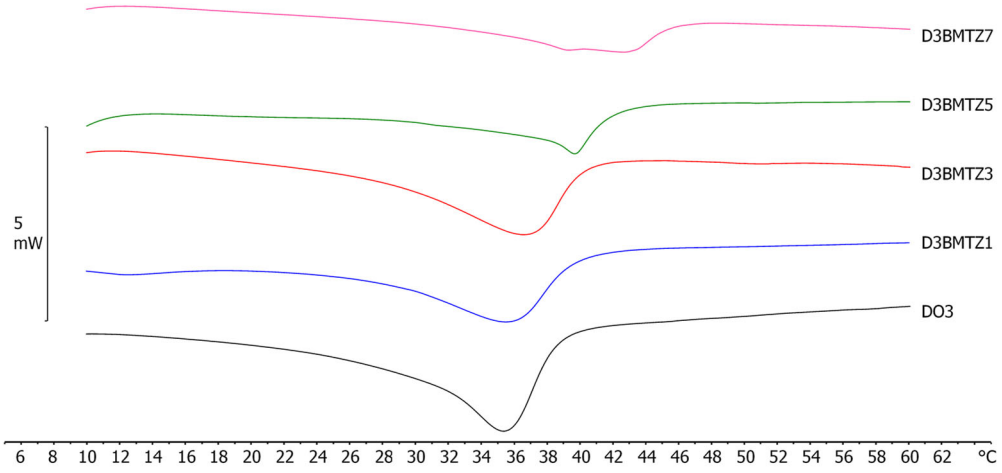

(**a**)

Figure 5. *Cont.*

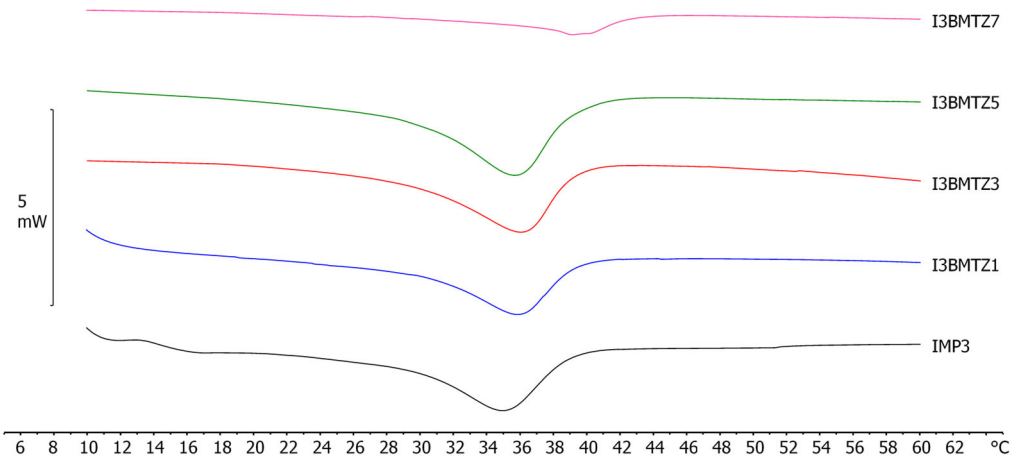

(**b**)

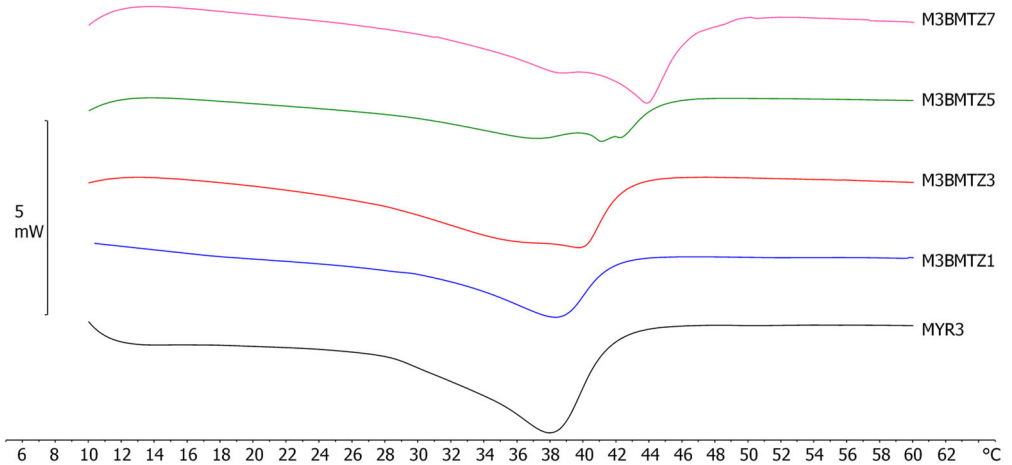

(**c**)

Figure 5. Curves obtained by differential scanning calorimetry of nanostructured lipid carriers (NLC) prepared using different percentages of bemotrizinol (BMTZ) and 3% *w*/*w* of the liquid lipid (**a**) decyl oleate (DO3 = unloaded NLC; DBMTZ1, DBMTZ3, DBMTZ5, and DBMTZ 7 loading 1, 3, 5, and 7% *w*/*w* BMTZ, respectively); (**b**) isopropyl myristate (IPM3 = unloaded NLC; IBMTZ1, IBMTZ3, IBMTZ5, and IBMTZ 7 loading 1, 3, 5, 7% *w*/*w* BMTZ respectively) and (**c**) caprilic/capric triglyceride (MYR3 = unloaded NLC; MBMTZ1, MBMTZ3, MBMTZ5, and MBMTZ 7 loading 1, 3, 5, and 7% *w*/*w* BMTZ, respectively).

Using IPM as liquid lipid, the incorporation of BMTZ up to 5% *w*/*w* led to small variations of the peak temperature and shape, while at 7% *w*/*w,* the calorimetric peak shifted to higher temperatures and its intensity decreased (Figure 5b). The presence of a single peak suggests that BMTZ settles uniformly in the NLC structure up to 5%. At higher amount, BMTZ does not distribute uniformly in the NLC matrix, as suggested by the presence of two peaks in the calorimetric curve.

The effect of loading BMTZ into NLC prepared using MYR was strongly dependent on the percentage of BMTZ (Figure 5c). The incorporation of BMTZ 1% *w*/*w* resulted in a slight increase in Tm and a lowering of ΔH. BMTZ 3% *w*/*w* led to the shift of the main peak to higher temperatures and the presence of a large shoulder at a temperature lower than that of the main peak. In the presence of BMTZ 5% *w*/*w*, the shoulder became a well-defined peak, and the main peak split into two peaks, both at higher temperatures.

When BMTZ was loaded at 7% *w*/*w*, all peaks moved to higher temperatures, and the central peak became the main one, whereas the right peak decreased turning into a shoulder. This behavior suggested a different location of BMTZ in the core of NLC prepared using MYR, depending on the percentage of BMTZ loaded.

Plotting the temperature variation of the NLC main peak as a function of the percentage of BMTZ loaded into the NLC, a different pattern was observed, depending on BMTZ concentration (Figure 6). At low BMTZ percentages (1–3% *w*/*w*), no appreciable difference was observed among the oils used to prepare NLC, while for NLC containing BMTZ 5–7% *w*/*w*, the increase in temperature of the mean peak was strongly dependent on the type of liquid lipid. The enthalpy variation (ΔH) and the percentage of recrystallization index (RI %) of NLC containing different percentages of BMTZ are listed in Table 7.

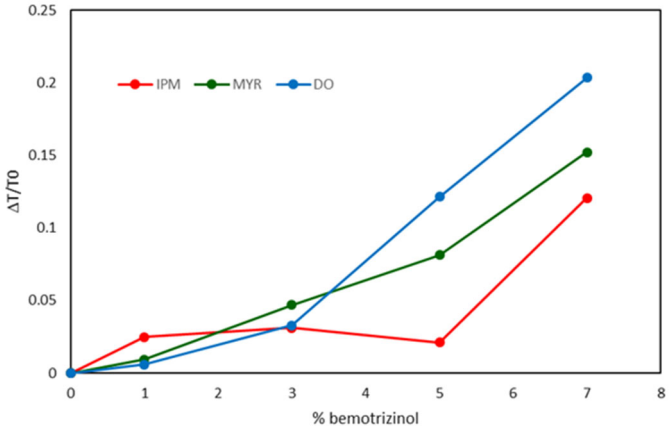

Figure 6. Peak temperature variation of nanostructured lipid carriers (NLC) prepared using isopropyl myristate (IPM), decyl oleate (DO), and caprilic/capric triglyceride (MYR) as a function of bemotrizinol (BMTZ) percentage. ($\Delta T = T - T_0$ where T is the peak temperature of BMTZ-loaded NLC and T_0 is the peak temperature of unloaded NLC). Peak temperature variation data were obtained from experiments performed in triplicate (n = 3) and their S.D. was within 1%.

Table 7. Enthalpy variation (ΔH) and percentage of recrystallization index (RI %) of nanostructured lipid carriers (NLC) containing 3% *w*/*w* liquid lipid, 4% *w*/*w* solid lipid, and different percentages of bemotrizinol.

NLC Code	ΔH ± S.D. (J/g)	RI %
DBMTZ1	2.72 ± 0.12	27.5
DBMTZ3	3.67 ± 0.13	37.1
DBMTZ5	2.03 ± 0.04	20.6
DBMTZ7	1.94 ± 0.09	19.6
IBMTZ1	2.00 ± 0.04	20.2
IBMTZ3	2.46 ± 0.11	24.8
IBMTZ5	2.93 ± 0.06	29.6
IBMTZ7	0.83 ± 0.03	8.4
MBMTZ1	2.10 ± 0.10	21.2
MBMTZ3	4.04 ± 0.12	40.9
MBMTZ5	2.58 ± 0.05	26.1
MBMTZ7	4.37 ± 0.21	44.2

From the calorimetric data, some hypotheses about the localization of BMTZ in the NLC structure could be put forward. In NLC containing DO, the variation of the peak temperature and RI % values suggest that BMTZ probably located preferentially in the solid lipid causing a stabilization of the ordered phase and a decrease in crystallinity. When IPM was used to prepare NLC, both the peak temperature and the crystallinity index

remained almost unaltered up to BMTZ 5% loading; this behavior could indicate that BMTZ preferentially locates among the liquid lipid molecules, leaving unaltered the solid lipid. At 7%, BMTZ could locate in the liquid lipid as well as in the solid lipid. As far as NLC containing MYR are concerned, multi-peak calorimetric curves, which were characterized by a temperature increase and a fluctuating crystallinity index, were observed; therefore, BMTZ could locate preferentially in the solid lipid in a non-uniform way, producing the stabilization of the ordered phase. The different distribution of BMTZ in the NLC core could affect both the stability and the loading capacity of the nanocarriers.

ζ-potential is regarded as a predictive parameter of the stability of colloidal systems. In particular, values of ζ-potential greater than 30 mV (as absolute value) are thought to be required for colloidal suspension stability [49]. As shown in Table 6, all BMTZ-loaded NLC had ζ-potential values close to −10 mV, thus suggesting poor stability of such colloidal carriers during storage. Stability studies pointed out that using DO or MYR as liquid lipid to prepare BMTZ-loaded NLC, a precipitate started forming one week after their preparation when BMTZ percentages greater than 3% w/w were loaded, while at lower BMTZ loading, the NLC remained clear up to two months of storage. The use of IPM allowed for obtaining BMTZ-loaded NLC that did not show any sign of precipitate after two months of storage at room temperature for all BMTZ percentages loaded into NLC. No relevant changes of mean size, PDI, and ζ-potential values were observed for BMTZ-loaded NLC that remained clear after two months of storage. This trend could suggest that the different chemical structure of the investigated lipids could account for the observed results. Indeed, cetyl palmitate and IPM are linear esters consisting of saturated chains, DO is a linear ester with an unsaturated chain, and MYR is a triglyceride. As cetyl palmitate and IPM have similar structures, a better interaction between these lipids could occur. As a result, a greater stability of lipid nanoparticles whose core consists of cetyl palmitate and IPM could be expected.

Previous studies on lipid nanoparticles prepared using the PIT method highlighted a good nanocarrier stability despite of ζ-potential values lower than 30 mV [30]. According to Stokes' law, another factor that could contribute to colloidal suspension stability was the particle size. However, the difference in particle sizes of the NLC under investigation could not account for the storage stability observed as BMTZ-loaded NLC having close sizes (e.g., IBMTZ7, MBMTZ5, and DBMTZ5) showed different stability. In a previous work [29], the good stability of NLC with ζ-potential values lower than 30 mV was attributed to a steric stabilization provided by the long polyoxyethylene chains of oleth-20 located on the surface of the nanoparticles. In addition to a likely steric stabilization, the results of the present study suggest that the different distribution of the active ingredient in the lipid matrix, highlighted by DSC data, may play a significant role in determining the stability of the nanoparticle suspension.

As NLC containing IPM proved stable at the highest percentage of BMTZ incorporation, this type of NLC was chosen to evaluate BMTZ loading capacity. This parameter was assessed as the maximum amount of BMTZ that could be encapsulated into NLC providing a colloidal suspension that did not show signs of precipitation, as already reported for other active ingredients [30,47]. When a water-insoluble compound, such as BMTZ, is incorporated into lipid nanoparticles, if the resulting colloidal dispersion is clear, the maximum amount of compound that could be present in the water phase of the colloidal suspension is the amount corresponding to its water solubility, while all compound is virtually in the lipid core of the nanocarrier. Therefore, when clear lipid nanoparticle dispersions were obtained, the entrapment efficiency was considered practically 100%. When BMTZ was incorporated into NLC prepared using IPM 3.0% w/w, a loading capacity as high as 8% w/w was achieved. As these nanoparticles showed mean size (190.6 ± 9.8 nm), PDI

(0.153 ± 0.013) and ζ-potential value (−10.6 ± 1.7 mV) suitable for the development of topical formulations, such NLC were incorporated into O/W emulsions. The same formulations containing analogous percentages of free BMTZ were prepared as control. The formulation free of BMTZ was coded A, formulations containing 0.4, 0.8, and 1.6% *w*/*w* free BMTZ were coded B, C, D, respectively. Formulations containing the corresponding amount of BMTZ loaded into NLC were coded B_{NLC}, C_{NLC}, and D_{NLC}.

All formulations showed good stability at room temperature as no significant changes of appearance, pH, and viscosity were observed at all sampling times.

As shown in Table 8, pH values of all investigated emulsions ranged from 6.5 to 7.5. Although the skin surface shows pH values in the range of 5.0–5.5, the investigated formulations could be regarded as safe as their pH value was close to the physiological one.

Table 8. pH, occlusion factor (F), spreadability (S), viscosity (V), cumulative amount of bemotrizinol released in vitro after 4 h (Q), and sun protection factor (SPF) of formulations containing free bemotrizinol or bemotrizinol-loaded nanostructured lipid carriers.

Emulsion Code	pH	F	S (cm)	V (cP)	Q (μg)	SPF
A	6.6 ± 0.1	50.41 ± 1.52	8.92 ± 0.31	27,200 ± 1200	---	1.22 ± 0.04
B	7.5 ± 0.2	53.31 ± 1.43	9.71 ± 0.22	26,500 ± 1400	0.60 ± 0.12	3.03 ± 0.11
B_{NLC}	7.0 ± 0.1	51.45 ± 0.99	10.33 ± 0.40	23,300 ± 900	0.98 ± 0.23	3.54 ± 0.12
C	7.4 ± 0.1	51.70 ± 1.32	8.73 ± 0.38	27,300 ± 1500	0.88 ± 0.17	4.14 ± 0.18
C_{NLC}	7.4 ± 0.2	49.83 ± 1.44	10.2 ± 0.14	23,900 ± 1100	0.87 ± 0.19	4.78 ± 0.21
D	7.5 ± 0.1	50.66 ± 0.98	9.32 ± 0.02	27,000 ±1400	0.71 ± 0.11	5.26 ± 0.28
D_{NLC}	7.4 ± 0.1	51.07 ± 1.02	10.8 ± 0.28	23,100 ± 1000	0.66 ± 0.13	6.34 ± 0.29

The incorporation of different percentages of BMTZ-loaded NLC into O/W emulsions led to a drop in viscosity and an increase in spreadability in comparison to the corresponding O/W emulsions containing free BMTZ. Plotting viscosity values vs. spreadability, an almost linear relationship (r^2 = 0.893) was observed (Figure 7), thus confirming the predictability of spreadability by measuring the viscosity of topical formulations [50,51].

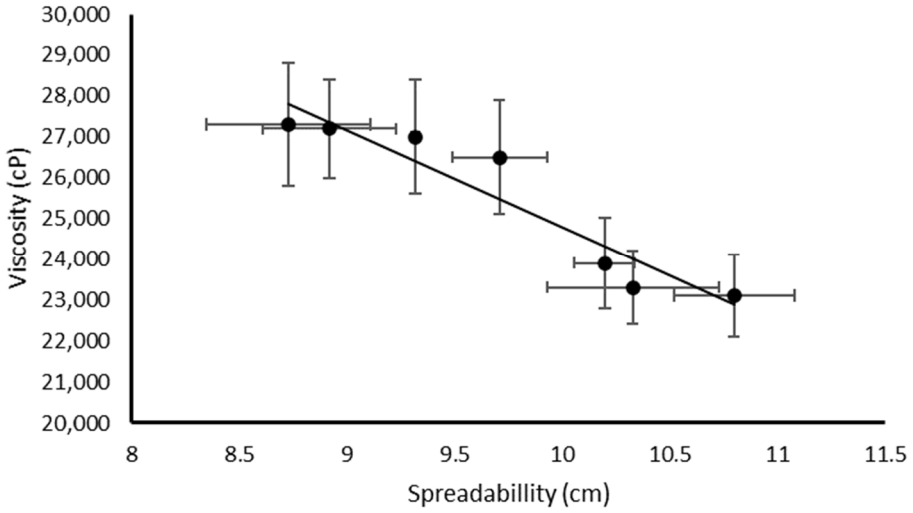

Figure 7. The relationship between viscosity and spreadability of O/W emulsions containing free bemotrizinol or nanostructured lipid carriers loaded with bemotrizinol.

As reported in the literature [52], the occlusive properties of O/W emulsions could be influenced by both the type and amount of oils used. The occlusive factors, reported in Table 8, pointed out a similar behavior of all investigated formulations, independently of the incorporation of different concentrations of BMTZ-loaded NLC or free BMTZ. No statistical difference among the occlusion factor values was observed ($p > 0.05$). According

to previous studies [35], the lower the crystallinity of lipid nanoparticles, the lower the occlusive properties. Therefore, the lack of any relevant effect on the occlusive factor of the NLC under investigation could be attributed to their low crystallinity resulting from their high content of liquid lipid. The stability of O/W emulsions stored at room temperature for three months was evaluated in terms of their appearance, pH, and viscosity. All formulations did not show significant variations in any of the three parameters.

BMTZ in vitro release from the formulations under investigation was expressed as cumulative amount released after 4 h because the sensitivity of the analytical method did not allow for BMTZ quantification in the period 0–3 h. Experiments lasted only 4 h because sunscreen products are not supposed to remain on the skin for longer periods. As shown in Table 8, no significant difference ($p > 0.05$) was observed comparing BMTZ release from formulations containing BMTZ-loaded NLC and free BMTZ. These results suggest that BMTZ delivery from the nanoparticles could not be regarded as the rate-limiting step in BMTZ release from the vehicle.

According to the literature [53,54], active ingredients loaded into lipid nanoparticles permeate mainly into the epidermis and the deeper layers of the skin while systemic absorption is restricted, thus avoiding undesired side effects. Assali and Zaid [55] reported that lipid nanoparticles having particle size above 100 nm and consisting of biodegradable materials could be regarded as safe. Therefore, the particle size (190.6 $\pm$ 9.8 nm) and safety of the solid/liquid lipids of the optimized BMTZ-loaded NLC investigated in this work suggest that topical application of these nanocarriers could not represent a risk for human health. In addition, in in vitro skin permeation experiments, no BMTZ could be detected after 4 h in the receiving compartment, thus supporting the safety of the investigated formulations. Other authors, performing a skin permeation study on BMTZ and other UV-filters, showed that no BMTZ permeation was observed after 24 h [56].

As shown in Table 8, BMTZ release from the emulsions under investigation was poor. However, the emulsion we used to perform in vitro release tests was not an optimized one but it was only a first formulation attempt to evaluate the effects of BMTZ-loaded NLC on the technological properties of the resulting emulsions. As the vehicle could strongly affect release and skin permeation of the active ingredient, we have planned further studies on O/W emulsions with different compositions and incorporating BMTZ-loaded NLC to assess the effects on BMTZ release and skin permeation from these vehicles.

As in vivo determination of SPF values of sunscreen formulations is expensive and time-consuming, different in vitro methods have been developed as alternative to in vivo tests in humans [57–60]. SPF values of the investigated formulations were determined the spectrophotometric method based on Mansur equation [39]. This type of test had already been applied to evaluate SPF values of emulsions containing active ingredients incorporated into lipid nanoparticles [61]. In the literature, the reliability of this spectrophotometric method has been debated owing to its poor ability to predict in vivo results, which was mainly attributed to an incorrect application of the method [62,63]. A recent study by Hermund et al. [64], compared the SPF values of three commercial sunscreen formulations obtained using the Mansur method with the SPF value reported by the manufacturer. A good agreement between claimed SPF and SPF values obtained by the Mansur equation was observed, thus underlining the usefulness of this in vitro method in the screening of sunscreen formulations during the development step.

In this work, the Mansur equation was used as a screening tool and its reliability was assessed comparing the obtained results with those determined in silico by the BASF sunscreen simulator (www.basf.com/sunscreen-simulator, accessed on 29 July 2025). This software has been developed based on the data reported by Ricci et al. [40] that conceptualize SPF in terms of areas under the transmittance vs. wavelength plots of sunscreen

products. The BASF sunscreen simulator predicted SPF values of 1.9, 2.7, and 4.2 for formulations containing 0.4, 0.8, and 1.6% *w*/*w* of free BMTZ, respectively. It is necessary to underline that this software cannot predict the vehicle effects.

As shown in Table 8, the emulsion without UV-filter provided a very low SPF value. The incorporation of a larger amount of free BMTZ raised the SPF value up to 5.3. These values were in good agreement with those predicted using the BASF sunscreen simulator, taking into account that the emulsion without UV-filter has an SPF value of 1.22. Formulations containing BMTZ loaded into NLC showed an improvement (about 20% for all investigated vehicles) of SPF value in comparison with the corresponding emulsions containing the same amount of free BMTZ. In particular, all formulations containing free BMTZ or BMTZ loaded into NLC showed SPF values that were significantly different ($p < 0.05$) compared with the blank emulsion. Statistically significant differences ($p < 0.05$) were observed for the following comparisons: emulsion B vs. emulsion B_{NLC}, emulsion C vs. emulsion C_{NLC}, and emulsion D vs. emulsion D_{NLC}. These results support the ability of NLC to behave as UV-blockers that has already been reported in the literature [35,59]. Therefore, incorporating BMTZ into suitable NLC could be a promising strategy to develop sunscreen formulations with reduced content of synthetic UV-filter while achieving higher SPF values. Further studies need to be performed to evaluate the in vivo sun protection factor of the investigated formulations to evaluate their actual potential in designing commercial sunscreen products.

4. Conclusions

The incorporation of different oils (decyl oleate, isopropyl myristate, and caprilic/capric triglyceride) into the lipid core of nanostructured lipid carriers (NLC) strongly affected the ability of such nanocarriers to load bemotrizinol (BMTZ), a broad-spectrum sunscreen agent. Differential calorimetry studies pointed out different interactions between BMTZ and the NLC core, depending on both the type and concentration of oil used. Among the investigated liquid lipids, isopropyl myristate provided the most stable NLC along with the greatest loading capacity for BMTZ (8% *w*/*w*). The incorporation of different percentages (5, 10, 20% *w*/*w*) of NLC loading 8% *w*/*w* BMTZ into O/W emulsions did not lead to relevant changes in pH, occlusion factor, spreadability, viscosity, and BMTZ in vitro release in the resulting formulations. On the contrary, vehicles containing BMTZ-loaded NLC showed about a 20% increase in the in vitro SPF value in comparison with the corresponding emulsions prepared using the same percentage of free BMTZ. These results suggest that the encapsulation of BMTZ into NLC could allow for improving the SPF value of the vehicle without increasing the amount of chemical UV-filter incorporated in the formulation. Therefore, loading BMTZ into properly designed NLC could be regarded as a useful tool to develop sunscreen products with improved safety and efficacy.

Supplementary Materials: The following supporting information can be downloaded at: https://www.mdpi.com/article/10.3390/colloids9050054/s1, Figure S1: Calorimetric curve, in heating mode, of cetyl palmitate; Figure S2: Calorimetric curve, in heating mode, of bemotrizinol.

Author Contributions: Conceptualization, M.G.S. and L.M.; methodology, M.G.S. and L.M.; validation, M.G.S., C.P. and L.M.; formal analysis, M.G.S. and L.M.; investigation, D.S., G.G. and S.R.; resources, M.G.S., C.P. and L.M.; data curation, M.G.S. and L.M.; writing—original draft preparation, M.G.S. and L.M.; writing—review and editing, M.G.S., D.S. and L.M.; visualization, M.G.S., D.S., G.G. and L.M.; supervision, L.M.; project administration, M.G.S., C.P. and L.M. All authors have read and agreed to the published version of the manuscript.

Funding: This research received no external funding.

Data Availability Statement: The data generated and/or analyzed during the current study are available from the corresponding author upon reasonable request.

Conflicts of Interest: The authors declare no conflicts of interest.

References

1. Lionetti, N.; Rigano, L. The New Sunscreens among Formulation Strategy, Stability Issues, Changing Norms, Safety and Efficacy Evaluations. *Cosmetics* **2017**, *4*, 15. [CrossRef]
2. Sander, M.; Sander, M.; Burbidge, T.; Beecker, J. The Efficacy and Safety of Sunscreen Use for the Prevention of Skin Cancer. *Can. Med. Assoc. J.* **2020**, *192*, E1802–E1808. [CrossRef] [PubMed]
3. Li, H.; Colantonio, S.; Dawson, A.; Lin, X.; Beecker, J. Sunscreen Application, Safety, and Sun Protection: The Evidence. *J. Cutan. Med. Surg.* **2019**, *23*, 357–369. [CrossRef]
4. Montenegro, L.; Turnaturi, R.; Parenti, C.; Pasquinucci, L. In Vitro Evaluation of Sunscreen Safety: Effects of the Vehicle and Repeated Applications on Skin Permeation from Topical Formulations. *Pharmaceutics* **2018**, *10*, 27. [CrossRef] [PubMed]
5. Ouchene, L.; Litvinov, I.V.; Netchiporouk, E. Systemic Absorption of Common Organic Sunscreen Ingredients Raises Possible Safety Concerns for Patients. *J. Cutan. Med. Surg.* **2019**, *23*, 449–450. [CrossRef]
6. Oral, D.; Yirun, A.; Erkekoglu, P. Safety Concerns of Organic Ultraviolet Filters: Special Focus on Endocrine-Disrupting Properties. *J. Environ. Pathol. Toxicol. Oncol.* **2020**, *39*, 201–212. [CrossRef]
7. Nesseem, D. Formulation of Sunscreens with Enhancement Sun Protection Factor Response Based on Solid Lipid Nanoparticles. *Int. J. Cosmet. Sci.* **2011**, *33*, 70–79. [CrossRef]
8. Nikolić, S.; Keck, C.M.; Anselmi, C.; Müller, R.H. Skin Photoprotection Improvement: Synergistic Interaction between Lipid Nanoparticles and Organic UV Filters. *Int. J. Pharm.* **2011**, *414*, 276–284. [CrossRef]
9. Khater, D.; Nsairat, H.; Odeh, F.; Saleh, M.; Jaber, A.; Alshaer, W.; Al Bawab, A.; Mubarak, M.S. Design, Preparation, and Characterization of Effective Dermal and Transdermal Lipid Nanoparticles: A Review. *Cosmetics* **2021**, *8*, 39. [CrossRef]
10. Chavda, V.P.; Acharya, D.; Hala, V.; Daware, S.; Vora, L.K. Sunscreens: A Comprehensive Review with the Application of Nanotechnology. *J. Drug Deliv. Sci. Technol.* **2023**, *86*, 104720. [CrossRef]
11. de Araújo, M.M.; Schneid, A.C.; Oliveira, M.S.; Mussi, S.V.; de Freitas, M.N.; Carvalho, F.C.; Bernes Junior, E.A.; Faro, R.; Azevedo, H. NLC-Based Sunscreen Formulations with Optimized Proportion of Encapsulated and Free Filters Exhibit Enhanced UVA and UVB Photoprotection. *Pharmaceutics* **2024**, *16*, 427. [CrossRef]
12. Sharma, B.; Chauhan, I.; Tiwari, R.K. Development of NLC-Based Sunscreen Gel of Green Tea Extract and Its In Vitro Characterization. *Curr. Bioact. Compd.* **2024**, *20*, 31–42. [CrossRef]
13. Paliwal, R.; Paliwal, S.R.; Kenwat, R.; Das Kurmi, B.; Sahu, M.K. Solid Lipid Nanoparticles: A Review on Recent Perspectives and Patents. *Expert. Opin. Ther. Pat.* **2020**, *30*, 179–194. [CrossRef] [PubMed]
14. Eroğlu, C.; Sinani, G.; Ulker, Z. Current State of Lipid Nanoparticles (SLN and NLC) for Skin Applications. *Curr. Pharm. Des.* **2023**, *29*, 1632–1644. [CrossRef]
15. Queiroz, M.d.C.V.; Muehlmann, L.A. Characteristics and Preparation of Solid Lipid Nanoparticles and Nanostructured Lipid Carriers. *J. Nanotheranostics* **2024**, *5*, 188–211. [CrossRef]
16. Pardeike, J.; Hommoss, A.; Müller, R.H. Lipid Nanoparticles (SLN, NLC) in Cosmetic and Pharmaceutical Dermal Products. *Int. J. Pharm.* **2009**, *366*, 170–184. [CrossRef]
17. Kakadia, P.; Conway, B. Lipid Nanoparticles for Dermal Drug Delivery. *Curr. Pharm. Des.* **2015**, *21*, 2823–2829. [CrossRef] [PubMed]
18. Kim, M.-H.; Jeon, Y.-E.; Kang, S.; Lee, J.-Y.; Lee, K.W.; Kim, K.-T.; Kim, D.-D. Lipid Nanoparticles for Enhancing the Physicochemical Stability and Topical Skin Delivery of Orobol. *Pharmaceutics* **2020**, *12*, 845. [CrossRef]
19. Tran, P.; Lee, S.-E.; Kim, D.-H.; Pyo, Y.-C.; Park, J.-S. Recent Advances of Nanotechnology for the Delivery of Anticancer Drugs for Breast Cancer Treatment. *J. Pharm. Investig.* **2020**, *50*, 261–270. [CrossRef]
20. Shirodkar, R.K.; Kumar, L.; Mutalik, S.; Lewis, S. Solid Lipid Nanoparticles and Nanostructured Lipid Carriers: Emerging Lipid Based Drug Delivery Systems. *Pharm. Chem. J.* **2019**, *53*, 440–453. [CrossRef]
21. Chatelain, E.; Gabard, B. Photostabilization of Butyl Methoxydibenzoylmethane (Avobenzone) and Ethylhexyl Methoxycinnamate by Bis-Ethylhexyloxyphenol Methoxyphenyl Triazine (Tinosorb S), a New UV Broadband Filter. *Photochem. Photobiol.* **2001**, *74*, 401. [CrossRef]
22. Teixeira Gomes, J.V.; Cherem Peixoto da Silva, A.; Lamim Bello, M.; Rangel Rodrigues, C.; Aloise Maneira Corrêa Santos, B. Molecular Modeling as a Design Tool for Sunscreen Candidates: A Case Study of Bemotrizinol. *J. Mol. Model.* **2019**, *25*, 362. [CrossRef]

23. Medeiros, T.S.; Moreira, L.M.C.C.; Oliveira, T.M.T.; Melo, D.F.; Azevedo, E.P.; Gadelha, A.E.G.; Fook, M.V.L.; Oshiro-Júnior, J.A.; Damasceno, B.P.G.L. Bemotrizinol-Loaded Carnauba Wax-Based Nanostructured Lipid Carriers for Sunscreen: Optimization, Characterization, and In Vitro Evaluation. *AAPS PharmSciTech* **2020**, *21*, 288. [CrossRef]
24. Wissing, S.A.; Müller, R.H. The Influence of the Crystallinity of Lipid Nanoparticles on Their Occlusive Properties. *Int. J. Pharm.* **2002**, *242*, 377–379. [CrossRef] [PubMed]
25. Souto, E.B.; Almeida, A.J.; Müller, R.H. Lipid Nanoparticles (SLN®, NLC®) for Cutaneous Drug Delivery:Structure, Protection and Skin Effects. *J. Biomed. Nanotechnol.* **2007**, *3*, 317–331. [CrossRef]
26. Subramaniam, B.; Siddik, Z.H.; Nagoor, N.H. Optimization of Nanostructured Lipid Carriers: Understanding the Types, Designs, and Parameters in the Process of Formulations. *J. Nanoparticle Res.* **2020**, *22*, 141. [CrossRef]
27. Anton, N.; Benoit, J.-P.; Saulnier, P. Design and Production of Nanoparticles Formulated from Nano-Emulsion Templates—A Review. *J. Control. Release* **2008**, *128*, 185–199. [CrossRef]
28. Safta, D.A.; Bogdan, C.; Moldovan, M.-L. SLNs and NLCs for Skin Applications: Enhancing the Bioavailability of Natural Bioactives. *Pharmaceutics* **2024**, *16*, 1270. [CrossRef]
29. Montenegro, L.; Santagati, L.M.; Sarpietro, M.G.; Castelli, F.; Panico, A.; Siciliano, E.A.; Lai, F.; Valenti, D.; Sinico, C. In Vitro Skin Permeation of Idebenone from Lipid Nanoparticles Containing Chemical Penetration Enhancers. *Pharmaceutics* **2021**, *13*, 1027. [CrossRef]
30. Sarpietro, M.G.; Torrisi, C.; Pignatello, R.; Castelli, F.; Montenegro, L. Assessment of the Technological Properties of Idebenone and Tocopheryl Acetate Co-Loaded Lipid Nanoparticles. *Appl. Sci.* **2021**, *11*, 3553. [CrossRef]
31. Ruktanonchai, U.; Limpakdee, S.; Meejoo, S.; Sakulkhu, U.; Bunyapraphatsara, N.; Junyaprasert, V.; Puttipipatkhachorn, S. The Effect of Cetyl Palmitate Crystallinity on Physical Properties of Gamma-Oryzanol Encapsulated in Solid Lipid Nanoparticles. *Nanotechnology* **2008**, *19*, 095701. [CrossRef]
32. Montenegro, L.; Rapisarda, L.; Ministeri, C.; Puglisi, G. Effects of Lipids and Emulsifiers on the Physicochemical and Sensory Properties of Cosmetic Emulsions Containing Vitamin E. *Cosmetics* **2015**, *2*, 35–47. [CrossRef]
33. Chaudhary, B.; Verma, S. Preparation and Evaluation of Novel in Situ Gels Containing Acyclovir for the Treatment of Oral Herpes Simplex Virus Infections. *Sci. World J.* **2014**, *2014*, 1–7. [CrossRef] [PubMed]
34. Elena, O.B.; Maria, N.A.; Michael, S.Z.; Natalia, B.D.; Alexander, I.B.; Ivan, I.K. Dermatologic Gels Spreadability Measuring Methods Comparative Study. *Int. J. Appl. Pharm.* **2022**, *14*, 164–168. [CrossRef]
35. Wissing, S.; Lippacher, A.; Müller, R. Investigations on the Occlusive Properties of Solid Lipid Nanoparticles (SLN). *J. Cosmet. Sci.* **2001**, *52*, 313–324.
36. Montenegro, L.; Parenti, C.; Turnaturi, R.; Pasquinucci, L. Resveratrol-Loaded Lipid Nanocarriers: Correlation between In Vitro Occlusion Factor and In Vivo Skin Hydrating Effect. *Pharmaceutics* **2017**, *9*, 58. [CrossRef] [PubMed]
37. Fallica, F.; Leonardi, C.; Toscano, V.; Santonocito, D.; Leonardi, P.; Puglia, C. Assessment of Alcohol-Based Hand Sanitizers for Long-Term Use, Formulated with Addition of Natural Ingredients in Comparison to WHO Formulation 1. *Pharmaceutics* **2021**, *13*, 571. [CrossRef]
38. Puglia, C.; Santonocito, D.; Bonaccorso, A.; Musumeci, T.; Ruozi, B.; Pignatello, R.; Carbone, C.; Parenti, C.; Chiechio, S. Lipid Nanoparticle Inclusion Prevents Capsaicin-Induced TRPV1 Defunctionalization. *Pharmaceutics* **2020**, *12*, 339. [CrossRef]
39. Mansur, J.S.; Breder, M.N.R.; Mansur, M.C.A.; Azulay, R.D. Determinação Do Fator de Proteção Solar Por Espectrofotometria. *An. Bras. Dermatol.* **1986**, *61*, 121–1245.
40. Ricci-Junior, E.; Dellamora Ortiz, G.M.; Pereira dos Santos, E.; de Carvalho Varjão Mota, A.; Antonio Ozzetti, R.; Luiz Vergnanini, A.; Santos-Oliveira, R.; Santos Silva, R.; Lira Ribeiro, V.; Maria Faria de Freitas, Z. In Vivo and in Vitro Evaluation of Octyl Methoxycinnamate Liposomes. *Int. J. Nanomed.* **2013**, *8*, 4689–4701. [CrossRef]
41. Fiume, M.M.; Bergfeld, W.F.; Belsito, D.V.; Hill, R.A.; Klaassen, C.D.; Liebler, D.C.; Marks, J.G.; Shank, R.C.; Slaga, T.J.; Snyder, P.W.; et al. Amended Safety Assessment of Triglycerides as Used in Cosmetics. *Int. J. Toxicol.* **2022**, *41*, 22–68. [CrossRef]
42. Fiume, M.M.; Heldreth, B.A.; Bergfeld, W.F.; Belsito, D.V.; Hill, R.A.; Klaassen, C.D.; Liebler, D.C.; Marks, J.G.; Shank, R.C.; Slaga, T.J.; et al. Safety Assessment of Alkyl Esters as Used in Cosmetics. *Int. J. Toxicol.* **2015**, *34*, 5S–69S. [CrossRef]
43. Gonzalez Solveyra, E.; Szleifer, I. What Is the Role of Curvature on the Properties of Nanomaterials for Biomedical Applications? *WIREs Nanomed. Nanobiotechnol.* **2016**, *8*, 334–354. [CrossRef]
44. Alajami, H.N.; Fouad, E.A.; Ashour, A.E.; Kumar, A.; Yassin, A.E.B. Celecoxib-Loaded Solid Lipid Nanoparticles for Colon Delivery: Formulation Optimization and In Vitro Assessment of Anti-Cancer Activity. *Pharmaceutics* **2022**, *14*, 131. [CrossRef] [PubMed]
45. Müller, R.H.; Mäder, K.; Gohla, S. Solid Lipid Nanoparticles (SLN) for Controlled Drug Delivery—A Review of the State of the Art. *Eur. J. Pharm. Biopharm.* **2000**, *50*, 161–177. [CrossRef] [PubMed]
46. Pardeshi, C.; Rajput, P.; Belgamwar, V.; Tekade, A.; Patil, G.; Chaudhary, K.; Sonje, A. Solid Lipid Based Nanocarriers: An Overview / Nanonosači Na Bazi Čvrstih Lipida: Pregled. *Acta Pharm.* **2012**, *62*, 433–472. [CrossRef]

47. Jenning, V.; Thünemann, A.F.; Gohla, S.H. Characterisation of a Novel Solid Lipid Nanoparticle Carrier System Based on Binary Mixtures of Liquid and Solid Lipids. *Int. J. Pharm.* **2000**, *199*, 167–177. [CrossRef]
48. Bunjes, H.; Westesen, K.; Koch, M.H.J. Crystallization Tendency and Polymorphic Transitions in Triglyceride Nanoparticles. *Int. J. Pharm.* **1996**, *129*, 159–173. [CrossRef]
49. Samimi, S.; Maghsoudnia, N.; Eftekhari, R.B.; Dorkoosh, F. *Characterization and Biology of Nanomaterials for Drug Delivery*; Elsevier: Amsterdam, The Netherlands, 2019; ISBN 9780128140314.
50. Lardy, F.; Vennat, B.; Pouget, M.P.; Pourrat, A. Functionalization of Hydrocolloids: Principal Component Analysis Applied to the Study of Correlations Between Parameters Describing the Consistency of Hydrogels. *Drug Dev. Ind. Pharm.* **2000**, *26*, 715–721. [CrossRef] [PubMed]
51. Garg, A.; Aggarwal, D.; Garg, S.; Singla, A.K. Spreading of Semisolid Formulations: An Update. *Pharm. Technol.* **2002**, *26*, 84–105.
52. Santonocito, D.; Puglia, C.; Montenegro, L. Effects of Lipid Phase Content on the Technological and Sensory Properties of O/W Emulsions Containing Bemotrizinol-Loaded Nanostructured Lipid Carriers. *Cosmetics* **2024**, *11*, 123. [CrossRef]
53. Ahmad, J. Lipid Nanoparticles Based Cosmetics with Potential Application in Alleviating Skin Disorders. *Cosmetics* **2021**, *8*, 84. [CrossRef]
54. Chu, C.C.; Hasan, Z.A.A.; Tan, C.P.; Nyam, K.L. In Vitro Safety Evaluation of Sunscreen Formulation from Nanostructured Lipid Carriers Using Human Cells and Skin Model. *Toxicol. Vitr.* **2022**, *84*, 105431. [CrossRef]
55. Assali, M.; Zaid, A.-N. Features, Applications, and Sustainability of Lipid Nanoparticles in Cosmeceuticals. *Saudi Pharm. J.* **2022**, *30*, 53–65. [CrossRef]
56. Souza, C.; Maia Campos, P.M.B.G. Development of a HPLC Method for Determination of Four UV Filters in Sunscreen and Its Application to Skin Penetration Studies. *Biomed. Chromatogr.* **2017**, *31*, e4029. [CrossRef] [PubMed]
57. Sheu, M.-T.; Lin, C.-W.; Huang, M.-C.; Shen, C.-H.; Ho, H.-O. Correlation of in Vivo and in Vitro Measurements of Sun Protection Factor. *J. Food Drug Anal.* **2003**, *11*, 12. [CrossRef]
58. Saraf, S.; Kaur, C. In Vitro Sun Protection Factor Determination of Herbal Oils Used in Cosmetics. *Pharmacogn. Res.* **2010**, *2*, 22. [CrossRef]
59. Pissavini, M.; Tricaud, C.; Wiener, G.; Lauer, A.; Contier, M.; Kolbe, L.; Trullás Cabanas, C.; Boyer, F.; Meredith, E.; de Lapuente, J.; et al. Validation of a New in Vitro Sun Protection Factor Method to Include a Wide Range of Sunscreen Product Emulsion Types. *Int. J. Cosmet. Sci.* **2020**, *42*, 421–428. [CrossRef] [PubMed]
60. Dimitrovska Cvetkovska, A.; Manfredini, S.; Ziosi, P.; Molesini, S.; Dissette, V.; Magri, I.; Scapoli, C.; Carrieri, A.; Durini, E.; Vertuani, S. Factors Affecting SPF in Vitro Measurement and Correlation with in Vivo Results. *Int. J. Cosmet. Sci.* **2017**, *39*, 310–319. [CrossRef]
61. Jose, J.; Netto, G. Role of Solid Lipid Nanoparticles as Photoprotective Agents in Cosmetics. *J. Cosmet. Dermatol.* **2019**, *18*, 315–321. [CrossRef] [PubMed]
62. Ácsová, A.; Hojerová, J.; Janotková, L.; Bendová, H.; Jedličková, L.; Hamranová, V.; Martiniaková, S. The Real UVB Photoprotective Efficacy of Vegetable Oils: In Vitro and in Vivo Studies. *Photochem. Photobiol. Sci.* **2021**, *20*, 139–151. [CrossRef] [PubMed]
63. Yang, S.I.; Liu, S.; Brooks, G.J.; Lanctot, Y.; Gruber, J. V Reliable and Simple Spectrophotometric Determination of Sun Protection Factor: A Case Study Using Organic UV Filter-Based Sunscreen Products. *J. Cosmet. Dermatol.* **2018**, *17*, 518–522. [CrossRef] [PubMed]
64. Hermund, D.B.; Torsteinsen, H.; Vega, J.; Figueroa, F.L.; Jacobsen, C. Screening for New Cosmeceuticals from Brown Algae Fucus Vesiculosus with Antioxidant and Photo-Protecting Properties. *Mar. Drugs* **2022**, *20*, 687. [CrossRef] [PubMed]